Acta Crystallographica Section F
Structural Biology and Crystallization Communications
ISSN 1744-3091

Crystallization and preliminary X-ray crystallographic analysis of the oxysterol-binding protein Osh3 from *Saccharomyces cerevisiae*

Junsen Tong,[a] Huiseon Yang,[a] Subin Ha,[a] Youngjin Lee,[b] Soo Hyun Eom[b] and Young Jun Im[a]*

[a]College of Pharmacy, Chonnam National University, Gwangju 500-757, Republic of Korea, and [b]Department of Life Science, Gwangju Institute of Science and Technology, Gwangju 500-712, Republic of Korea

Correspondence e-mail: imyoungjun@jnu.ac.kr

Received 7 August 2012
Accepted 10 October 2012

Oxysterol-binding protein (OSBP) related proteins (ORPs) are conserved from yeast to humans and are implicated in regulation of sterol homeostasis and in signal transduction pathways. Osh3 of *Saccharomyces cerevisiae* is a pleckstrin-homology (PH) domain-containing ORP member that regulates phosphoinositide metabolism at endoplasmic reticulum–plasma membrane contact sites. The N-terminal PH domain of Osh3 was purified and crystallized as a lysozyme fusion and the resulting crystal diffracted to 2.3 Å resolution. The crystal belonged to the monoclinic space group $C2$, with unit-cell parameters $a = 98.03$, $b = 91.31$, $c = 84.13$ Å, $\beta = 81.41^\circ$. With two molecules in the asymmetric unit, the Matthews coefficient was 3.13 Å^3 Da^{-1}. Initial attempts to solve the structure by molecular-replacement techniques using T4 lysozyme as a search model were successful. The C-terminal OSBP-related domain (OBD) of Osh3 was crystallized by the vapour-diffusion method and the resulting crystal diffracted to 1.5 Å resolution. The crystal was orthorhombic, belonging to space group $P2_12_12_1$, with unit-cell parameters $a = 41.57$, $b = 87.52$, $c = 100.58$ Å. With one molecule in the asymmetric unit, the Matthews coefficient was 2.01 Å^3 Da^{-1}. Initial attempts to solve the structure by the single-wavelength anomalous dispersion technique using bromine were successful.

1. Introduction

Oxysterol-binding protein (OSBP) and its related proteins (ORPs) constitute a large family of lipid-binding proteins that are evolutionarily conserved from yeast to humans. They are implicated in many cellular processes including cell signalling, vesicular trafficking, lipid metabolism and nonvesicular lipid transport (Raychaudhuri & Prinz, 2010). The deletion of all seven ORPs (*OSH1–OSH7*) in yeast is lethal, with severe defects in sterol and lipid distribution. However, the expression of any one *OSH* gene restores viability, indicating that all of the homologues share at least one essential function (Beh *et al.*, 2001; Beh & Rine, 2004).

Humans have 12 ORP genes and splicing variations further increase the number of different protein products (Lehto *et al.*, 2001). ORPs can be divided into two subtypes: 'long' and 'short' homologues. A common feature of all ORPs is a conserved C-terminal OSBP-related ligand-binding domain (ORD) which contains the highly conserved 'OSBP fingerprint (motif)' sequence EQVSHHPP. ORD has been shown to bind sterols and phosphatidylinositol 4-phosphate (PI4P) in the same binding pocket (Im *et al.*, 2005; de Saint-Jean *et al.*, 2011). Short ORPs comprise only a ligand-binding ORD with little additional sequence. Long ORPs contain additional N-terminal variable regions such as the GOLD domain, ankyrin repeats, pleckstrin-homology (PH) domain and FFAT motif (Ngo *et al.*, 2010). The PH domains of various ORPs have been found to bind phosphoinositides and to mediate the localization of ORP proteins. The FFAT motif serves as a targeting determinant for the endoplasmic reticulum by interacting with vesicle-associated membrane-protein-associated protein (VAP) homologues (Loewen *et al.*, 2003). The ankyrin repeats and the GOLD domain mediate protein–protein interactions (Ngo *et al.*, 2010).

One of the well known functions of ORPs is nonvesicular lipid transport between membranes. Both long and short ORPs can be enriched at membrane-contact sites, junctions of the endoplasmic reticulum with other organelles, where it is suggested that they execute regulatory or lipid-transfer functions (Schulz *et al.*, 2009; Vihervaara, Jansen *et al.*, 2011). Yeast Osh4 has been shown to exchange sterols for PI4P between lipid bilayers (de Saint-Jean *et al.*, 2011). There is much evidence to suggest that some ORPs act as sterol regulators or sensors that relay information to a spectrum of different cellular processes. Human OSBP1 is a cholesterol-sensing regulator of two protein phosphatases: PTPPBS and the serine/threonine phosphatase PP2A (Wang *et al.*, 2005). Oxysterol binding changes the subcellular localization of OSBP1, ORP1L and ORP2, suggesting a sterol-sensor action of these ORPs (Ridgway *et al.*, 1992; Vihervaara, Jansen *et al.*, 2011). ORP1L forms a complex with Rab7 GTPase and the effector protein RILP. Sterol binding by ORP1L regulates late endosome distribution and motility (Vihervaara, Uronen *et al.*, 2011). Yeast Osh proteins (Osh3–Osh7) act as controllers of PI4P signalling and metabolism by regulating SacI phosphatase activity at membrane-contact sites (Stefan *et al.*, 2011).

The structure of a small yeast ORP homologue Osh4 revealed that the core of the protein consists of an almost complete β-barrel and three α-helices with a ligand-binding tunnel (Im *et al.*, 2005). The ORD binds a single molecule of a lipid such as cholesterol, ergosterol, oxysterols or PI4P that shields the hydrophobic acyl chains from the aqueous environment (Im *et al.*, 2005; de Saint-Jean *et al.*, 2011). Currently, Osh4 is the only ORP homologue with a known three-dimensional structure. Since the sequence identity of Osh4 to the ORD domains of long ORP members is low (14–33% identity) and the functions of the ORP members are diverse, the extrapolation of the structural features of Osh4 to other ORPs is limited. The major challenge is to unravel how the ligand binding by ORD domains is integrated with the various functions of ORPs. In addition, the mechanistic relationship between the N-terminal domains and the ORD is still not clearly known. For these reasons, we initiated crystallographic studies of yeast Osh3 in order to establish a representative structural context of a long ORP member. Here, we report the crystallization and X-ray data collection of the Osh3 PH domain and ORD from *Saccharomyces cerevisiae* and the preliminary trials for structure determination.

2. Materials and methods

2.1. Cloning and protein expression

DNA encoding the PH domain (residues 221–317) and ORD (residues 605–996) of Osh3 (UniProt ID P38713) was amplified by polymerase chain reaction using *S. cerevisiae* genomic DNA as a template. The primers for Osh3 PH were 5′-GATACACCATGGGTCGTTACTTGCAAGGC-3′ (forward) and 5′-GATACACTCGAGTCACTGATCGTCAAAACAAGTTTG-3′ (reverse). The primers for Osh3 ORD were 5′-GTAATATGGATCCGAGCGCCCAATCCTCAACAG-3′ (forward) and 5′-GATACACTCGAGTCACTGATCGTCAAAACAAGTTTG-3′ (reverse). The PCR products of each domain were subcloned into the *Nco*I/*Xho*I and *Bam*HI/*Xho*I sites of modified pHIS-2 and pGEX-4T vectors, respectively. Osh3 PH was tagged with an N-terminal hexahistidine followed by a thrombin protease cleavage site (LVPR/GS). PH domain with an N-terminal His tag or a glutathione S-transferase (GST) tag was insoluble. In order to increase the solubility of the PH-domain construct and to facilitate structure determination by molecular replacement, a tripeptide (KRL) in the $\beta1$–$\beta2$ loop (residues 234–236) was replaced by bacteriophage T4 lysozyme (residues 2–161). The T4 lysozyme had C54T/C97A mutations for the prevention of cysteine-residue oxidation (Matsumura *et al.*, 1989). Expression of the PH domain fused with the active T4 lysozyme resulted in poor cell growth and a low protein yield. Therefore, a D20N mutation was introduced into the active site of the T4 lysozyme to prevent bacterial cell lysis upon protein expression. For the lysozyme insertion, a DNA sequence corresponding to amino-acid residues 234–236 of the PH domain was mutated to a *Sal*I restriction-enzyme recognition sequence. The lysozyme PCR products with overhanging *Sal*I restriction sites at the 5′ and 3′ ends were digested with *Sal*I and ligated into the *Sal*I site in the PH domain. Osh3 ORD was tagged with an N-terminal hexahistidine and GST followed by a tobacco etch virus (TEV) protease cleavage site (ENLYFQ/G). *Escherichia coli* strain BL21(DE3) Star cells transformed with the plasmids encoding the PH domain and ORD were grown to an OD_{600} of 0.8 at 310 K in LB medium. Cells were induced by the addition of IPTG to a final concentration of 0.5 m*M* and were incubated for 12 h overnight at 293 K prior to harvesting.

2.2. Purification

For the purification of the PH-lysozyme protein, pelleted cells were resuspended in 2× PBS buffer containing 20 m*M* imidazole and lysed by sonication. The supernatant containing His-tagged PH-lysozyme was applied onto an Ni–NTA affinity column. The fusion protein was eluted from the column using 100 m*M* Tris–HCl pH 8.0, 300 m*M* imidazole. The eluate was concentrated to 10 mg ml^{-1} and the His tag was removed by cleavage with thrombin protease. Subsequently, the sample was subjected to size-exclusion chromatography on a Superdex 200 column (GE Healthcare) equilibrated with 20 m*M* Tris–HCl pH 8.0, 300 m*M* NaCl, 10 m*M* β-mercaptoethanol. The fractions containing PH-lysozyme were concentrated to 12 mg ml^{-1} for crystallization. Protein concentrations were measured based on the absorption of light at 280 nm using extinction coefficients of 1.61 and 1.60 mg ml^{-1} cm^{-1} for the PH-lysozyme and ORD, respectively. Cells expressing Osh3 ORD were resuspended in 2× PBS buffer containing 20 m*M* imidazole and lysed by sonication. The supernatant containing His-GST-ORD was applied onto an Ni–NTA affinity column. The fusion protein was eluted from the column using 100 m*M* Tris–HCl pH 8.0, 300 m*M* imidazole. The eluate was concentrated to 10 mg ml^{-1} and the His-GST tag was removed by cleavage with TEV protease. The Osh3 ORD was separated from His-GST by HiTrap SP ion-exchange chromatography. The fractions containing Osh3 ORD were subjected to size-exclusion chromatography on a Superdex 200 column (GE Healthcare) equilibrated with 20 m*M* Tris–HCl pH 8.0, 150 m*M* NaCl. The fractions containing the Osh3 ORD were concentrated to 10 mg ml^{-1} for crystallization.

2.3. Crystallization of Osh3 PH and ORD

Preliminary crystallization experiments for the PH domain and ORD were carried out at 295 K in 96-well crystallization plates using a multichannel pipette and customized crystallization screening solutions by dispensing 0.8 µl protein solution and 0.8 µl precipitant solution. Initial crystals of the PH domain appeared after 2 d using a solution consisting of 0.1 *M* Tris–HCl pH 8.0, 15% PEG 8000, 0.2 *M* Li_2SO_4. The condition was further optimized in order to obtain crystals suitable for X-ray analysis. A drop consisting of 1.2 µl protein solution was mixed with 1.2 µl precipitant solution and equilibrated against 1 ml reservoir solution consisting of 0.1 *M* Tris–HCl pH 8.0, 15% PEG 6000, 0.2 *M* $MgSO_4$ using the hanging-drop technique in 15-well screw-cap plates. High-quality crystals with dimensions of

0.15 × 0.15 × 0.02 mm grew in 2 d (Fig. 1). Initial crystals of Osh3 ORD appeared after 5 d using a solution consisting of 0.1 *M* HEPES–NaOH pH 7.0, 25% PEG 1500, 0.2 *M* $MgCl_2$. The crystallization condition was further optimized to 0.1 *M* MES–NaOH pH 6.0, 25% PEG 1500, 0.1 *M* $MgCl_2$ using the hanging-drop technique in 15-well screw-cap plates. A drop consisting of 2 µl protein solution was mixed with 2 µl precipitant solution and equilibrated against 1 ml reservoir solution. High-quality crystals with dimensions of 0.1 × 0.1 × 0.15 mm appeared in one week. In order to obtain derivatized crystals for heavy-atom phasing, 0.2 *M* NaBr and 0.1 m*M* $KAu(CN)_2$ were added to the crystallization buffer and crystals were grown by microseeding techniques.

2.4. Diffraction experiment

Crystals of the PH domain and ORD were cryoprotected in reservoir solution supplemented with 10% glycerol and flash-cooled by immersion in liquid nitrogen. Crystals were preserved in a cryogenic N_2-gas stream (∼100 K) during diffraction experiments.

Diffraction data for native Osh3 PH-lysozyme were collected at a fixed wavelength of 0.97949 Å using an ADSC Q315 CCD detector on the 5C beamline at Pohang Light Source (PLS), Pohang Accelerator Laboratory, Republic of Korea. Diffraction data for native Osh3 ORD were collected at a fixed wavelength of 0.91997 Å using an ADSC Q315 CCD detector on the BL17U1 beamline at the SSRF, People's Republic of China; a typical diffraction pattern is shown in Fig. 2. For structure determination, single-wavelength anomalous dispersion (SAD) data from bromine-labelled crystals were collected at the peak wavelength of 0.91950 Å on the AR-NW12A beamline at the Photon Factory (PF), Japan using an ADSC Q210 CCD detector. All data were processed and scaled using *HKL*-2000 (Otwinowski & Minor, 1997) and handled with the *CCP*4 program suite (Winn *et al.*, 2011). SAD phasing was performed with the program *SOLVE* (Terwilliger & Berendzen, 1999) and density modification was performed using *RESOLVE* (Terwilliger, 2000).

3. Results and discussion

For crystallographic studies of the Osh3 PH domain, we tested expression of the PH domain with two different domain boundaries (residues 200–317 and residues 221–317), which were cloned into vectors providing hexahistidine, His-tagged maltose-binding protein or GST N-terminal tags. However, all of the PH-domain constructs were insoluble when expressed in *E. coli*. Homology modelling of the Osh3 PH domain using the solution structure of ORP11 PH (PDB entry 2d9x; RIKEN Structural Genomics/Proteomics Initiative, unpublished work) indicated that nine of the 13 residues in the $\beta1$–$\beta2$ loop (residues 229–242) were lysine or arginine, forming a strongly electropositive surface. We speculated that the clustering of many basic residues on one face of the PH domain might lead to the poor solubility on *E. coli* overexpression. To attenuate and to cover the strongly basic surface, T4 lysozyme was inserted into the $\beta1$–$\beta2$ loop replacing a tripeptide (KRL; residues 234–236) in the PH domain (residues 221–317). The replacement of an internal flexible loop by a globular domain might be advantageous in crystallization by providing new rigid lattice contacts. The internal lysozyme fusion is expected to have lower entropy in hinge movement between domains than fusing the lysozyme to the N- or C-termini of the target protein. This technique of T4 lysozyme fusion to a flexible loop has successfully been exploited in the crystallographic studies of several GPCR receptors (Rosenbaum *et al.*, 2007; Chien *et al.*, 2010). The PH domain fused with T4 lysozyme in the $\beta1$–$\beta2$ loop was solubly expressed with an N-terminal hexahistidine tag and was purified to homogeneity. However, a PH domain with a T4 lysozyme fusion in the $\beta3$–$\beta4$ loop replacing the tetrapeptide HNQT (residues 260–263) was still insoluble. The fusion protein was crystallized and the resulting crystal

Table 1
Summary of diffraction data statistics.

Values in parentheses are for the highest resolution shell.

Crystal	PH	ORD (native)	ORD (NaBr)
Construct	Residues 221–317	Residues 605–996	Residues 605–996
Wavelength (Å)	0.97949	0.91997	0.91950 [peak]
X-ray source	5C, PLS	BL17U1, SSRF	AR-NW12A, PF
Space group	*C*2	$P2_12_12_1$	$P2_12_12_1$
Unit-cell parameters (Å)	a = 98.0, b = 91.3, c = 84.13	a = 40.9, b = 89.2, c = 96.1	a = 41.6, b = 87.5, c = 100.6
Resolution (Å)	2.3 (2.34–2.30)	1.5 (1.53–1.50)	1.9 (1.93–1.90)
No. of unique reflections	32983	56991	29751
Multiplicity	3.3 (3.0)	7.1 (5.9)	14.6 (14.8)
$\langle I/\sigma(I)\rangle$	23.2 (3.5)	40.0 (4.6)	54.3 (12.8)
$R_{\rm merge}$† (%)	6.7 (30.8)	8.8 (34.3)	7.0 (26.9)
Data completeness (%)	99.4 (98.7)	99.7 (99.4)	99.9 (100.0)

† $R_{\rm merge} = \sum_{hkl}\sum_i |I_i(hkl) - \langle I(hkl)\rangle| / \sum_{hkl}\sum_i I_i(hkl)$, where $I_i(hkl)$ is the observed intensity and $\langle I(hkl)\rangle$ is the average intensity of multiple observations of symmetry-related reflections.

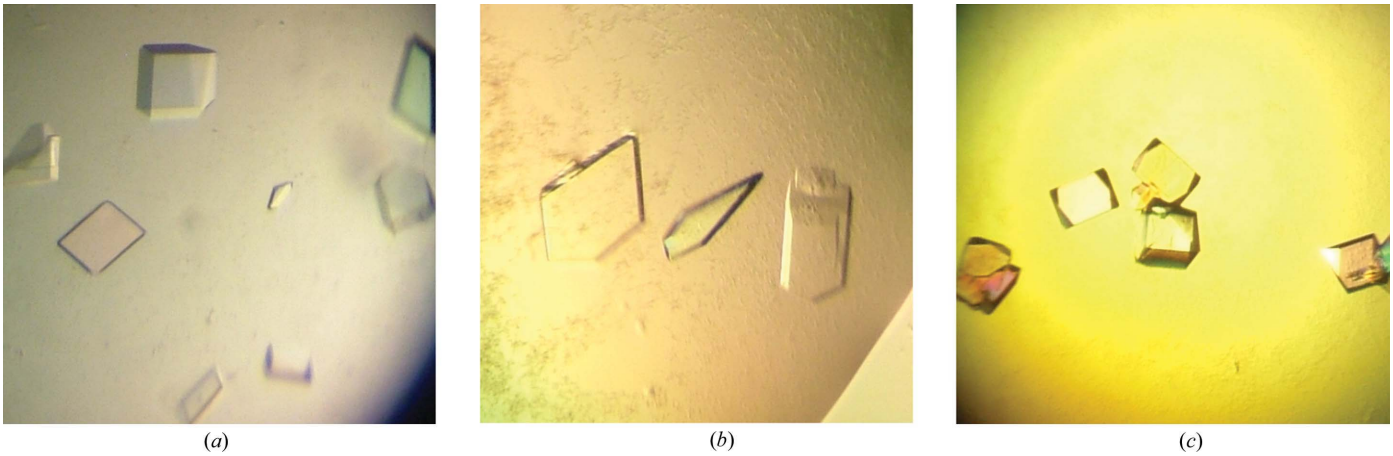

(*a*) (*b*) (*c*)

Figure 1
Crystals of the PH domain and ORD of Osh3 from *S. cerevisiae*. (*a*) Native crystals of Osh3 PH–T4 lysozyme fusion protein with typical dimensions of 0.15 × 0.15 × 0.02 mm. (*b*) Native crystals of Osh3 ORD with typical dimensions of 0.2 × 0.2 × 0.01 mm obtained using 0.1 *M* MES pH 6.0, 25% PEG 1500, 0.1 *M* $MgCl_2$. (*c*) Bromine-labelled Osh3 ORD crystals with dimensions of 0.1 × 0.1 × 0.1 mm obtained in a condition consisting of 0.1 *M* MES pH 6.0, 25% PEG 1500, 0.1 *M* $MgCl_2$, 0.2 *M* NaBr, 0.1 m*M* $KAu(CN)_2$.

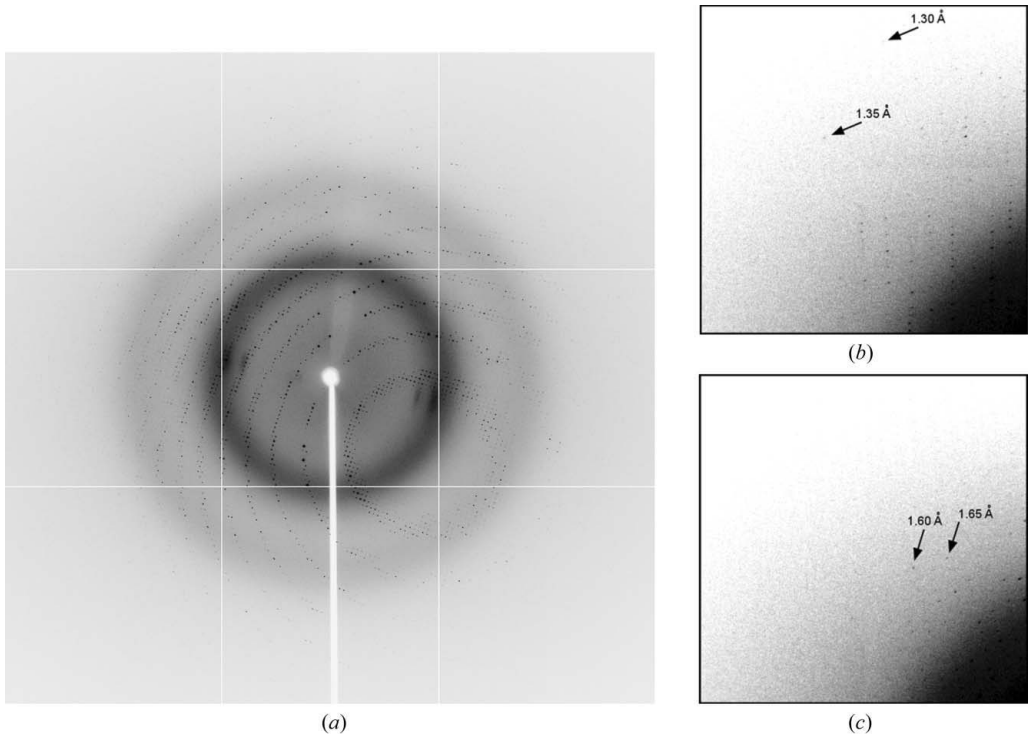

Figure 2
(*a*) A typical diffraction image of an Osh3 ORD crystal with an oscillation angle of 1°. The image was obtained at an ω angle at 90° (rotational axis). Images were collected from a single cryocooled crystal with a crystal-to-detector distance of 200 mm using a wavelength of 0.91950 Å. The edges of the detector correspond to a d_{min} of 1.45 Å. (*b*) The first diffraction image of an Osh3 ORD crystal (ω angle of 0°). The upper left portion of the diffraction image (1/9 of the image area) is shown. (*c*) The last diffraction image of the Osh3 ORD crystal (ω angle of 199°).

diffracted to 2.3 Å resolution. The crystal belonged to the monoclinic space group *C*2, with unit-cell parameters a = 98.03, b = 91.31, c = 84.13 Å, β = 81.41°. With two molecules in the asymmetric unit, the Matthews coefficient (Matthews, 1968) was 3.13 Å^3 Da^{-1} (solvent content 60.75%). The lysozyme fusion provided an advantage in determining phase information by molecular replacement. Two molecules of T4 lysozyme (PDB entry 212l; Vetter *et al.*, 1996) were found in the asymmetric unit using the program *MOLREP* (Vagin & Teplyakov, 2010) and the density-modified map showed clear electron densities of PH domains which were not included in the search model.

The Osh3 ORD was cloned with tandem hexahistidine and GST N-terminal affinity tags. The fusion protein was expressed in *E. coli* BL21(DE3) Star cells. The His-GST fusion to Osh3 ORD provided substantially higher expression and solubility than a His-tag fusion. Complete diffraction data sets for Osh3 ORD were collected to 1.5 Å resolution from a native crystal and to 1.9 Å resolution for a SAD data set from a bromine-labelled crystal. The native crystal initially diffracted to 1.3 Å resolution. However, owing to a decay in crystal quality by radiation damage during data collection, data processing was limited to 1.5 Å resolution (Fig. 2). Data-collection statistics are shown in Table 1. Analysis of the diffraction intensities confirmed the space group to be orthorhombic $P2_12_12_1$, with unit-cell parameters a = 41.57, b = 87.52, c = 100.58 Å, for the native crystals. With one molecule in the asymmetric unit, the calculated Matthews coefficient was 2.01 Å^3 Da^{-1}, corresponding to a solvent content of 38.94%. Br-SAD phasing was carried out using the program *SOLVE* at 1.9 Å resolution. A total of 23 bromine sites were found by an automated heavy-atom search, with a figure of merit of 0.34. The phases were further improved by density modification using the program *RESOVE*. The resulting electron-density map with a figure of merit of 0.67 was readily interpretable. Automated model building using the program *RESOLVE* covered 60% of the amino-acid sequence of Osh3 ORD. The structures of the Osh3 PH domain and ORD are expected to provide key structural information that is conserved in long OSBP members.

We are grateful to the staff members at beamline 5C of Pohang Light Source, Republic of Korea for their assistance. We would like to thank the beamline staff at BL17U1 of the SSRF and at AR-NW12A of the Photon Factory. This project was supported by a National Research Foundation of Korea (NRF) grant funded by the Korean government (grant No. 2011-0025110) and the intramural research program of Chonnam National University to YJI (2010).

References

Beh, C. T., Cool, L., Phillips, J. & Rine, J. (2001). *Genetics*, **157**, 1117–1140.
Beh, C. T. & Rine, J. (2004). *J. Cell Sci.* **117**, 2983–2996.
Chien, E. Y., Liu, W., Zhao, Q., Katritch, V., Han, G. W., Hanson, M. A., Shi, L., Newman, A. H., Javitch, J. A., Cherezov, V. & Stevens, R. C. (2010). *Science*, **330**, 1091–1095.
Im, Y. J., Raychaudhuri, S., Prinz, W. A. & Hurley, J. H. (2005). *Nature (London)*, **437**, 154–158.
Lehto, M., Laitinen, S., Chinetti, G., Johansson, M., Ehnholm, C., Staels, B., Ikonen, E. & Olkkonen, V. M. (2001). *J. Lipid Res.* **42**, 1203–1213.
Loewen, C. J., Roy, A. & Levine, T. P. (2003). *EMBO J.* **22**, 2025–2035.
Matsumura, M., Becktel, W. J., Levitt, M. & Matthews, B. W. (1989). *Proc. Natl Acad. Sci. USA*, **86**, 6562–6566.
Matthews, B. W. (1968). *J. Mol. Biol.* **33**, 491–497.
Ngo, M. H., Colbourne, T. R. & Ridgway, N. D. (2010). *Biochem. J.* **429**, 13–24.
Otwinowski, Z. & Minor, W. (1997). *Methods Enzymol.* **276**, 307–326.
Raychaudhuri, S. & Prinz, W. A. (2010). *Annu. Rev. Cell Dev. Biol.* **26**, 157–177.
Ridgway, N. D., Dawson, P. A., Ho, Y. K., Brown, M. S. & Goldstein, J. L. (1992). *J. Cell Biol.* **116**, 307–319.

Rosenbaum, D. M., Cherezov, V., Hanson, M. A., Rasmussen, S. G. F., Thian, F. S., Kobilka, T. S., Choi, H.-J., Yao, X.-J., Weis, W. I., Stevens, R. C. & Kobilka, B. K. (2007). *Science*, **318**, 1266–1273.
Saint-Jean, M. de, Delfosse, V., Douguet, D., Chicanne, G., Payrastre, B., Bourguet, W., Antonny, B. & Drin, G. (2011). *J. Cell Biol.* **195**, 965–978.
Schulz, T. A., Choi, M.-G., Raychaudhuri, S., Mears, J. A., Ghirlando, R., Hinshaw, J. E. & Prinz, W. A. (2009). *J. Cell Biol.* **187**, 889–903.
Stefan, C. J., Manford, A. G., Baird, D., Yamada-Hanff, J., Mao, Y. & Emr, S. D. (2011). *Cell*, **144**, 389–401.
Terwilliger, T. C. (2000). *Acta Cryst.* D**56**, 965–972.
Terwilliger, T. C. & Berendzen, J. (1999). *Acta Cryst.* D**55**, 1872–1877.
Vagin, A. & Teplyakov, A. (2010). *Acta Cryst.* D**66**, 22–25.
Vetter, I. R., Baase, W. A., Heinz, D. W., Xiong, J.-P., Snow, S. & Matthews, B. W. (1996). *Protein Sci.* **5**, 2399–2415
Vihervaara, T., Jansen, M., Uronen, R. L., Ohsaki, Y., Ikonen, E. & Olkkonen, V. M. (2011). *Chem. Phys. Lipids*, **164**, 443–450.
Vihervaara, T., Uronen, R. L., Wohlfahrt, G., Bjorkhem, I., Ikonen, E. & Olkkonen, V. M. (2011). *Cell. Mol. Life Sci.* **68**, 537–551.
Wang, P., Weng, J. & Anderson, R. G. W. (2005). *Science*, **307**, 1472–1476.
Winn, M. D. *et al.* (2011). *Acta Cryst.* D**67**, 235–242.